arXiv:1805.03466v1 [astro-ph.EP] 9 May 2018

EVIDENCE OF A SUB-SATURN AROUND EPIC 211945201

Abhijit Chakraborty,[1] Arpita Roy,[2] Rishikesh Sharma,[1] Suvrath Mahadevan,[3,4]
Priyanka Chaturvedi,[1] Neelam J.S.S.V Prasad,[1] and B. G. Anandarao[1]

[1]*Astronomy & Astrophysics Division, Physical Research Laboratory, Ahmedabad 380009, India*
[2]*Department of Astronomy, California Institute of Technology, Pasadena, CA 91125, USA*
[3]*Department of Astronomy & Astrophysics, The Pennsylvania State University, University Park, PA 16802, USA*
[4]*Center for Exoplanets and Habitable Worlds, The Pennsylvania State University, University Park, PA 16802, USA*

ABSTRACT

We report here strong evidence for a sub-Saturn around EPIC 211945201 and confirm its planetary nature. EPIC 211945201b was found to be a planetary candidate from *K2* photometry in Campaigns 5 & 16, transiting a bright star (V_{mag} = 10.15, G0 spectral type) in a 19.492 day orbit. However, the photometric data combined with false positive probability calculations using VESPA was not sufficient to confirm the planetary scenario. Here we present high-resolution spectroscopic follow-up of the target using the PARAS spectrograph (19 radial velocity observations) over a time-baseline of 420 days. We conclusively rule out the possibility of an eclipsing binary system and confirm the 2-σ detection of a sub-Saturn planet. The confirmed planet has a radius of 6.12±0.1 $R_\oplus$, and a mass of $27^{+14}_{-12.6}$ $M_\oplus$. We also place an upper limit on the mass (within the 3-σ confidence interval) at 42 $M_\oplus$ above the nominal value. This results in the Saturn-like density of $0.65^{+0.34}_{-0.30}$ g cm^{-3}. Based on the mass and radius, we provide a preliminary model-dependent estimate that the heavy element content is 60-70 % of the total mass. This detection is important as it adds to a sparse catalog of confirmed exoplanets with masses between 10-70 $M_\oplus$ and radii between 4-8 $R_\oplus$, whose masses and radii are measured to a precision of 50% or better (only 23 including this work).

1. INTRODUCTION

A large number of transiting exoplanets have been discovered by dedicated space based photometric missions such as *CoRoT* (Baglin et al. 2006), *Kepler* (Borucki et al. 2010) and *K2* (Howell et al. 2014), and then followed up with ground-based spectroscopic resources for mass measurement using the radial velocity (RV) technique. However, the canon is limited in the number of exoplanets with radii between 2-8 $R_\oplus$ that also have masses measured with a precision of 50% or better. Subse-

Corresponding author: Abhijit Chakraborty
abhijit@prl.res.in

quently, this has limited our understanding of the composition, evolutionary history, and diversity of a population of exoplanets that have been variously defined as super-Neptunes (10-40 $M_\oplus$ and 2-6 $R_\oplus$, Barragán et al. 2016) or sub-Saturns (10-70 $M_\oplus$ and 4-8 $R_\oplus$, Petigura et al. 2017).

In the absence of precise mass measurements, or rather prior to the engagement of ground-based spectroscopic resources, there are still confidence levels that can be placed on the detection of an exoplanet candidate. Statistical validation tools such as BLENDER (Torres et al. 2011), PASTIS (Díaz et al. 2014), and VESPA (Morton 2012), can give higher confidence in the planetary scenerio than false positive alternatives by calculating the authenticity of the transit signal, in conjunction with ancillary information about the system, using a Bayesian approach. For example, recent work by Mayo et al. (2018) confirmed 149 exoplanets and identified 275 planetary candidates (PC) based on the false positive probabilities (FPP) of the transit signature. However, there remain sources whose transit signals are inadequate to confirm the nature of the system – these are essential candidates for follow-up with high-precision RV spectrographs. Combining the photometry with RV data allows us to determine the mass and radius of the exoplanet, and hence its density. Theories of internal structure and planet formation mechanism are increasingly better constrained as we expand the number of exoplanets with precise measurements of mass and radius (Lopez & Fortney 2014, and references therein). Hence ground-based radial velocity follow-up for mass determination, although quite resource-limited, remains of extreme importance for understanding exoplanet demographics.

In this paper, we report evidence for the sub-Saturn nature of EPIC 211945201b, a planetary candidate observed in *K2* Campaigns 5 & 16. In Sections 2 & 3 we present the *K2* photometry and the analysis of archival Keck *K*-band imaging data. Section 4 elaborates on the statistical validation procedures of the PC using the VESPA framework. In Section 5 we describe our follow-up campaign with the PARAS spectrograph and the corresponding RV analysis. Section 6 reports our final host star properties, and Section 7 describes the simultaneous fitting of RV and photometric data. We discuss our results in Section 8 and conclude in Section 9.

2. *K2*-PHOTOMETRY

The NASA *K2* mission (Howell et al. 2014) observed the source EPIC 211945201 from 27 April 2015 to 10 July 2015 (73 days) & 07 December 2017 to 25 February 2018 (81 days) as a part of Campaign 5 and Campaign 16, respectively. This target was identified as a transiting planetary candidate system by Pope et al. (2016), Barros et al. (2016), Petigura et al. (2018) and Mayo et al. (2018) using the light curve from Campaign 5, while Yu et al. (2018) recently used campaign 16 data to declare it a high quality planetary candidate.

There have been several pipelines developed to correct the systematics from the *K2* light curve. Examples include `k2sff` (Vanderburg & Johnson 2014), `k2sc` (Aigrain et al. 2016), `k2phot` (Aigrain et al. 2016) & the `everest` package (Luger et al. 2016). All the works identifying the possible planetary nature of EPIC 211945201b, referred to above, used one of above pipelines to extract and correct the light curve. In general, they first corrected the light curve and then searched for the significant transit signature using the `BLS` (Kovács et al. 2002) algorithm. In the BLS algorithm, the transit event is modeled as a box shaped modulation of the light curve. Following this approach, the occurrence of a single transit event was found at 19.49179 days (Mayo et al. 2018) from Campaign 5, and at 19.492036 days (Yu et al. 2018) from Campaign 16, which are both consistent within their error bars.

We retrieved the `K2PHOT` light curves (Petigura et al. 2015; Aigrain et al. 2016) for both campaigns through ExoFOP[1] – these are shown in Fig 1. Seven transits, three in the upper panel & four in the lower panel, spaced every ~ 19.49 days, are clearly visible in the light curve of EPIC 211945201. In this work we use the combined light curve of both Campaigns 5 & 16, and adopt a period of 19.49215 days from its analysis (see §7).
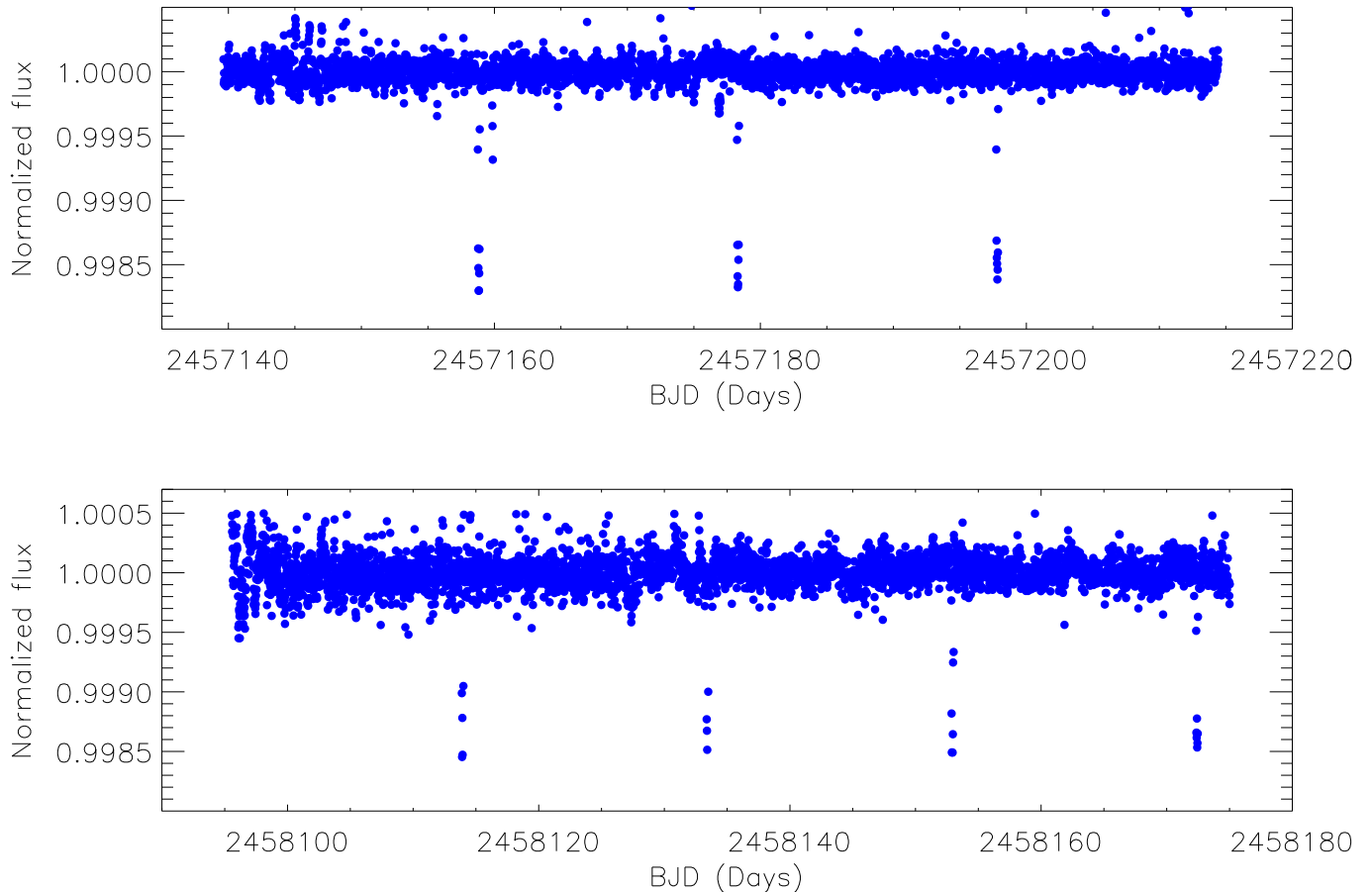

Figure 1. `K2PHOT` photometry data of EPIC 211945201. The upper panel shows the light curve from Campaign 5 (≈ 73 d), while the lower panel light curve is from Campaign 16 (≈ 81 d). Three transits in Campaign 5, and four transits in Campaign 16 are clearly visible for this target.

3. HIGH ANGULAR RESOLUTION IMAGING

High-resolution imaging is an immensely useful tool for constraining the probability of blended background objects. We made use of the archival high angular resolution AO imaging data acquired using the Keck II/NIRC2 camera. This is also publicly available on ExoFOP (uploaded by user David Ciardi). The Keck AO data was obtained on January 21st of 2016(UT) with a K-band filter. NIRC2 has a pixel scale of $0.009942''$/pixel. The observed image and 5-σ sensitivity curve are shown
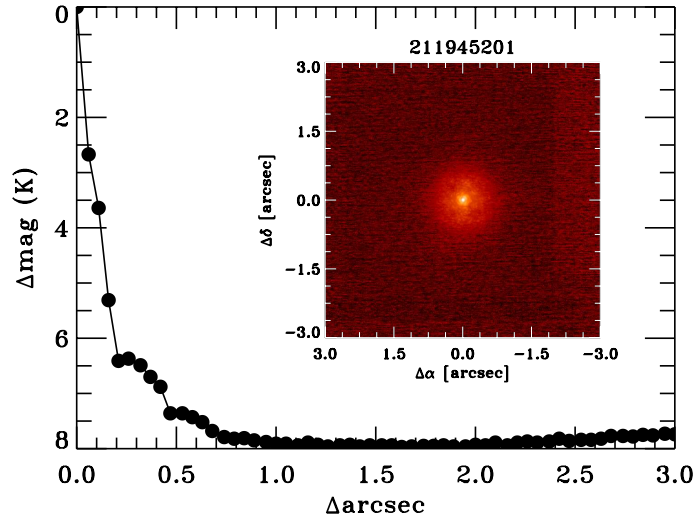
---

[1] https://exofop.ipac.caltech.edu/k2/

Figure 2. High angular resolution image of the source EPIC 211945201, and the 5-σ sensitivity/contrast curve curve in K-band observed with the NIRC2 instrument on the 10m Keck II telescope (publicly available on ExoFOP, contributed by user David Ciardi).

in Fig 2. The star appears single and has no close companions within the several arcseconds. At a separation of 0.5″the estimated sensitivity to the companion is ≈ 8 mag. This effectively rules out the possibility of background sources within this separation contributing significant flux to the light curve. The estimated point spread function (PSF) of the source is 0.0526″.

4. STATISTICAL VALIDATION

We used the open source and publicly available VESPA[2] package from Morton (2012, 2015), to determine the FPP (False Positive Probabilities) of the transit signature. The code uses transit parameters like shape, depth, and duration of each transit event, as well as independent observational constraints (like AO imaging for example) to validate the transit signal of a planet. VESPA uses TRILEGAL (TRIdimensional modeL of thE GALaxy) to simulate the population of each possible false positive scenario (such as background eclipsing binary, eclipsing binary, hierarchical eclipsing binary etc.) in a particular part of the sky using the coordinates of the source. It uses this population set combined with the observational constraints/priors to calculate the prior for each scenario, and then the likelihood of the each scenario. The resultant numbers are used to calculate a final probability for the validation of each contamination scenario.

VESPA requires certain inputs before calculating the FPP, such as aperture size used for the extraction of the light curve, secondary eclipse threshold, and photometric and spectroscopic parameters of the host star. Here the default aperture size used for extraction of K2PHOT light curve (Petigura et al. 2015; Aigrain et al. 2016) is supplied to constrain the maximum allowed separation between the target and the source of the transit event. A search for the secondary eclipse was also undertaken using the method described in Dressing et al. (2017), between values of 0.3-0.8 in orbital phase. It was found that the existing data could exclude events deeper than 5×10^{-5} in units of the normalized flux. This value is then used by VESPA as a limit on the allowable secondary eclipse. High resolution contrast curves can also be supplied to constrain the authenticity of transit signal. The Keck

---

[2] https://github.com/timothydmorton/VESPA

K-band contrast curve (§3) along with other publicly available contrast curves like Gemini r-band and Gemini z-band[3] acquired using NIRI (Hodapp et al. 2003) are supplied as input. These contrast curves are especially useful for the validation process as they can preclude the presence of nearby or background stars above a certain brightness at a given distance on sky.
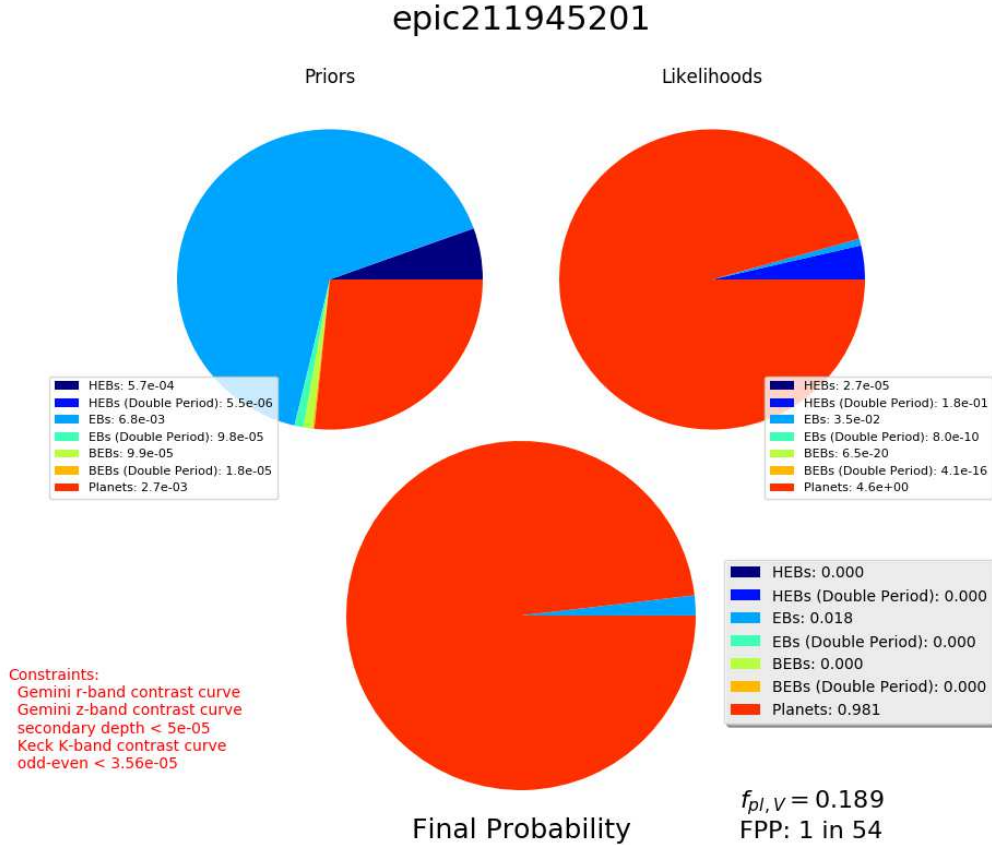

Figure 3. False Positive Probability (FPP) analysis using the `VESPA` package from Morton (2012, 2015). The incorporates the prior likelihood of a false positive scenario (given sky position, AO-imaging contrast curve data, and wavelength-dependent magnitudes), with the likelihood of the transit photometry under various scenarios. The results shown here are obtained by using the combined light curve of EPIC 211945201 from Campaigns 5 & 16.

The properties of the host star from ExoFOP (e.g. coordinates, magnitudes in various bands, see Huber et al. 2016) and other parameters summarized in Table 1, were also supplied as input. The values of spectroscopic properties (mainly temperature, surface gravity and metallicity) used for the FPP calculations were obtained through spectral analysis of data obtained with the PARAS spectrograph and are listed in Table 3 and further discussed in Section 6.

We performed the `VESPA` analysis separately for Campaign 5 & Campaign 16 data and found the probability for the planetary scenario to be $\sim$87% & $\sim$96%, and the false positive probability (FPP) to be $\sim$13% & $\sim$4% respectively. We note that much of this work was initially motivated by the individual results of Campaign 5, which were much less supportive of the planetary interpretation.

---

[3] Also retrieved from ExoFOP, uploaded by David Ciardi

Table 1. Stellar parameters supplied for Fpp calulations

Parameters	Value	source
Main identifiers		
α(J2000)(hh:mm:ss)	09:06:17.75	EPIC
δ(J2000)(Degrees)	19:24:08.11	EPIC
2MASS	J09061775 + 1924080	EPIC
EPIC	211945201	EPIC
TYC	1404-1186-1	EPIC
Magnitudes		
B	10.937±0.080	EPIC
g	10.479±0.030	EPIC
V	10.154±0.056	EPIC
r	10.038±0.040	EPIC
Kep	10.115	EPIC
i	9.959±0.080	EPIC
J	9.144±0.023	2MASS
H	8.908±0.028	2MASS
K	8.837±0.020	2MASS
W1	8.822±0.023	WISE
W2	8.844±0.020	WISE
W3	8.810±0.028	WISE
W4	8.623±0.398	WISE

NOTE—Parameters with source flagged as EPIC are taken from the Ecliptic Plane Input Catalogue available at http://archive.stsci.edu/k2/epic/search.php. Other parameters whose sources are flagged as 2MASS and WISE are taken from (Cutri et al. 2003) and (Cutri & et al. 2013), respectively.

Ultimately we used the combined light curve from both the campaigns to calculate a probability of ∼98% (Fig 3) for the planetary scenario, with the remaining ∼2% probability attributed to an eclipsing binary (EB) scenario. The threshold for planetary validation is a stringent < 1% FPP (Crossfield et al. 2016), which relegated EPIC 211945201 to the status of planetary candidate, despite the coverage of multiple transit events. Since the results of the FPP calculation from VESPA could not single-handedly rule out the possibility of an EB, follow up with high-precision Doppler spectroscopy was necessary to establish the planetary nature of the candidate.

5. SPECTROSCOPIC FOLLOW-UP OBSERVATIONS

In order to confirm the planetary nature of the candidate, high-resolution ($R \sim 67,000$) spectroscopic follow-up observations were undertaken with the PARAS spectrograph (Chakraborty et al. 2014) mounted on a 1.2 meter telescope at Gurushikhar Observatory, Mount Abu, India. PARAS is a fiber-fed, temperature and pressure stabilized, white pupil echelle spectrometer that has earlier been shown to achieve ~ 1 m s^{-1} RV precision on timescales of a month (Roy et al. 2016). A total of 19 spectra were acquired between 25th November 2016 and 18th January 2018 using the simultaneous wavelength calibration mode (using a ThAr hollow cathode lamp) as explained in Chakraborty et al.

(2014). Besides science exposures, five bias frames and three flat frames were also acquired on each night in order to correct the bias & verify the cross-dispersed order locations on the stabilized instrument. After each science exposure ThAr-ThAr exposures were also acquired, illuminating both the science and calibration fiber with the ThAr lamp, to correct the instrumental as well as inter-fiber drift. More details of the spectrograph, observational procedure, and data analysis techniques are described in Chakraborty et al. (2014). The source was observed only in dark (moon-less) and photometric sky conditions. The airmass for all the epochs were <1.5 and seeing was better than 1.5". The exposure time for each observation was between 1800s−3000s as the source is towards the fainter limit of PARAS (see Table 2) which resulted in signal-to-noise ratios (SNR) between 13 to 20 per pixel at the blaze peak wavelength of 5500 Å. A list of epochs and observational details is shown in Table 2. The first column in the table represents observation time stamp in terms of BJD-TDB. The observed RV values are listed in the next column followed by the RV errors, which are based on both photon noise and the fitting errors of the cross correlation function (CCF; for CCF error estimations see Chaturvedi et al. 2016a). The RV data spans more than a year – nearly 420 days.

5.1. *RV analysis*

The entire data reduction and RV analysis for PARAS was carried out by the automated pipeline in IDL based on the REDUCE optimal extraction routines of Piskunov & Valenti (2002) and explained in Chakraborty et al. (2014). In order to reduce the data, the pipeline performs routine tasks like bias subtraction, order trace verification, cosmic ray correction (especially important due to the deep depletion CCD in PARAS), and optimal extraction of both target and calibration spectra. Instrumental drifts are tracked and corrected by cross-correlation of the simultaneous calibration spectrum with a custom ThAr mask made for the PARAS lamp. RVs are derived by cross-correlating the target spectra with a suitable numerical stellar template mask. The stellar mask is created from a synthetic spectrum of the star, containing the majority of deep photospheric absorption lines. See Baranne et al. (1996), Pepe et al. (2002) and references therein for a more detailed description of the mask cross-correlation method. Based on the temperature given in Table 3, which is determined from spectral analysis (see Sec 6), our source is found to be a F9/G0 spectral type star. Thus, we use a G2-type stellar mask for cross-correlation of the spectra. RV measurement errors, which are given in Table 2, are based on photon noise errors (Bouchy et al. 2001) and the errors associated with the CCF fitting function. These errors range from 9 to 16 m s^{-1}; the method for their computation is described in Chaturvedi et al. (2016a).

The radial velocities from PARAS are plotted in Fig. 6, along with the best fit model (determined by the joint fit with the photometric data) described in Sec 7. In order to check radial velocity variation induced by a blended spectrum, we computed the bisector inverse slope (BIS) of the cross-correlation function for each observation in the manner of Queloz et al. (2001). The value of the BIS for each CCF, and its respective errors, are listed in Table 2 and plotted in Fig 7. We find no correlation between the bisector inverse slope and the measured radial velocity. If the signal detected was due to a blended spectrum, then we would expect to see a strong correlation between the bisector slopes and radial velocity measurements (e.g. Wright et al. 2013).

5.2. *Discarding an EB scenerio*

The radial velocities observed with PARAS are listed in Table 2 and plotted in Fig 4. The change in the RV values throughout our observational span is small – within ±20 m s^{-1} – which discards

the possibility that this is an EB system. The RV dataset combined with FPP results (Sec 4) shows very strong evidence that the body revolving around EPIC 211945201 in a 19.491 day orbit is indeed a planet.

Table 2. Radial Velocities of EPIC 211945201 in chronological order

BJD_{TDB}	RV	σ-RV	BIS	σ-BIS	Exp. Time
	(km s^{-1})	(km s^{-1})	(km s^{-1})	(km s^{-1})	(sec.)
2457717.469599	1.2657	0.0087	0.1763	0.0105	3000
2457755.352017	1.2698	0.0088	-0.0437	0.0155	3000
2457756.343921	1.2613	0.0089	-0.0066	0.0110	3000
2457757.300892	1.2607	0.0098	0.3477	0.0102	3000
2457757.344621	1.2678	0.0088	0.3419	0.0132	3000
2457758.348027	1.2567	0.0097	0.1885	0.0099	3000
2457761.483625	1.2594	0.0098	-0.0853	0.0112	3000
2457761.522539	1.2597	0.0086	-0.1513	0.0107	3000
2457786.395919	1.2501	0.0086	0.1565	0.0080	2400
2457787.435365	1.2610	0.0098	-0.1214	0.0086	2400
2457790.417556	1.2487	0.0098	0.0058	0.0099	2400
2457815.206300	1.2687	0.0123	0.3546	0.0244	1800
2457816.230661	1.2671	0.0124	0.1758	0.0239	1800
2457818.178771	1.2704	0.0121	0.1407	0.0127	1800
2457843.222090	1.2525	0.0150	0.0891	0.0148	2400
2458080.433400	1.2528	0.0151	0.1871	0.1255	2400
2458083.416314	1.2720	0.0129	0.0690	0.1746	2400
2458111.447097	1.2606	0.0102	0.1629	0.0422	2400
2458137.379171	1.2628	0.0136	0.7929	0.1392	2400

To verify the instrument stability of the PARAS spectrograph over the same period of time, the RV standard star HD55575 (Bouchy et al. 2013) was monitored closely alongside EPIC 211945201. This star was observed by SOPHIE (Bouchy et al. 2013; Perruchot et al. 2008) in HR+ mode for a span of 118 days. The RV dispersion (σ_{RV}) of this target was reported to be 3.4 m s^{-1} in Bouchy et al. (2013). We acquired 58 spectra of HD55575 over a span of 391 days. The RVs were then calculated identical to the manner described in Sec 5.1 for EPIC 211945201. The σ_{RV} with PARAS was found to be 3.5 m s^{-1}. Nightly binning of the data points reduced this dispersion further to 3.1 m s^{-1}. This demonstrates that our RV dispersion is consistent with that achieved by SOPHIE for HD55575, and quantifies the upper limit of the spectrograph's stability during the entire long span of observations of EPIC 211945201. With strong evidence that our source hosts an exoplanet, we proceed to estimating the mass of the transiting body by simultaneous modeling of RV and photometry data in the Sec 7.
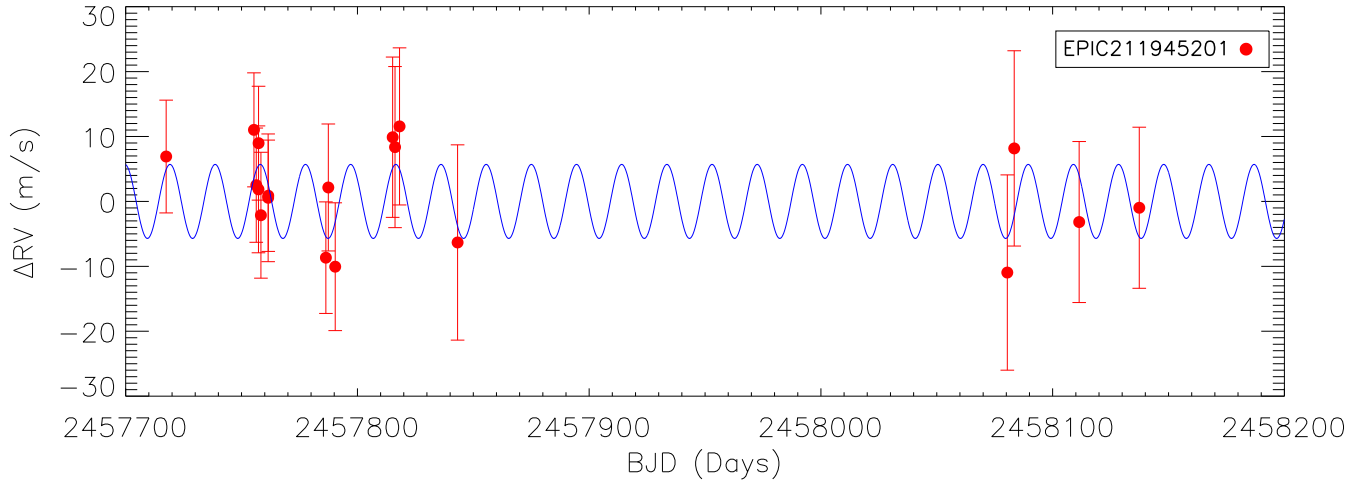
6. PHYSICAL PARAMETERS OF THE STAR

Figure 4. Radial velocities for EPIC 211945201 over a span of 420 days, observed with the PARAS spectrograph. The absence of large RV dispersion is clearly seen, which discards an EB scenario(see Sec 5.2). The overlaid blue curve is the best fit model to our dataset (from PYANETI).
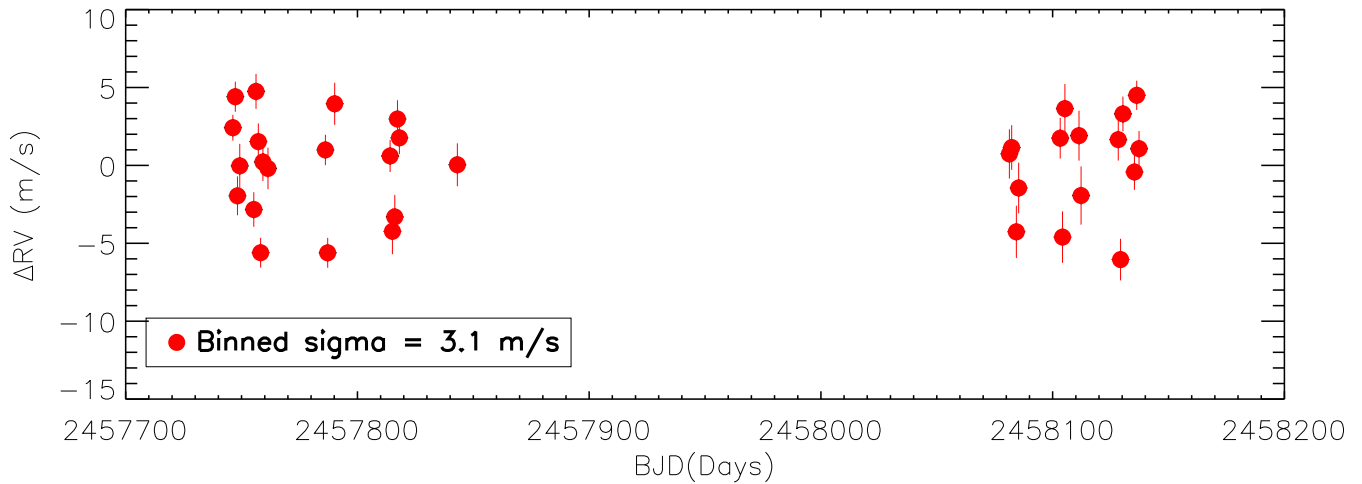

Figure 5. Radial velocities for standard star HD55575. The RV points in red show nightly binned averages. The data spans over 391 days and demonstrates instrument stability and performance during the acquisition of the EPIC 211945201 data.

The spectral parameters of the star were first estimated using the `PARAS SPEC` package (Chaturvedi et al. 2016a). `PARAS SPEC` is a stellar synthesis pipeline that estimates $T_{\rm eff}$, $\log(g)$, $[Fe/H]$, $vsini$ & $v_{\rm micro}$ by implementing both synthetic spectral fitting and equivalent width mea-

Table 3. Stellar parameters

Parameters	(Petigura et al. 2018)	(Mayo et al. 2018)	This work
$T_{\rm eff}$[K]	6018±60	6046±50	6025±100
$\log(g)$[dex]	4.13±0.1	4.14±0.1	4.25±0.1
[Fe/H][dex]	0.12±0.04	0.05±0.08	0.1±0.1
$v_{\rm micro}$ [Km/s]	-	-	0.4±0.1
$v_{\rm rot}$ [Km/s]	3.3±1.0	-	4.0±1.0

surements. The details of the package can be found in Chaturvedi et al. (2016a) & Chaturvedi et al. (2016b). For EPIC 211945201, the coadded high SNR spectra for all the epochs listed in Table 2 were used for this analysis. The adopted values for stellar parameters are the weighted average of the results obtained from both the methods of PARAS SPEC. Stellar parameters present in the literature, along with our new estimates, are listed in Table 3. It can be seen that our estimated parameters are within the 2-σ confidence interval of the parameters available in the literature. These estimated stellar parameters, along with the photometric magnitudes given in Table 1 of the star in different bands, are used to derive the physical parameters of the star. The new precision astrometry from the GAIA DR2 data release (Gaia Collaboration et al. 2018) is also used in this derivation of stellar parameters. The parallax for the star measured by GAIA is 5.475±0.039[4]. The Dartmouth Stellar evolution database (Dotter et al. 2008) is utilized to obtain the radius, mass, age and distance to the host star using the ISOCHRONE package (Morton 2015). The uncertainties associated with photometric and spectroscopic observables were also taken into account while estimating the properties of the star. Finally, a radius of $R_* = 1.38^{+0.017}_{-0.018}\ R_\odot$, mass of $M_* = 1.18^{+0.03}_{-0.04}\ M_\odot$, age of $3.99^{+0.85}_{-0.7}$ Gyr, and a distance of 182.6±1.3 pc are determined for the star. The very precise parallax measurements from GAIA lead to an extremely precise determination of stellar parameters, shrinking the error bars by an order of magnitude, and exhibiting the tremendous value of this mission.

7. SIMULTANEOUS FITTING AND MODELING OF RV AND PHOTOMETRY DATA

The *K2* photometry data and PARAS radial velocity data are simultaneously fitted using the PYANETI routine of (Barragán et al. 2016, 2017). This PYTHON code uses Markov chain Monte Carlo (MCMC) methods with a Bayesian approach and a parallelized ensemble sampler algorithm in Fortran. The photometric dataset included in the joint analysis was subset of the whole k2sff light curve. About 13 hours of data centered on each of the seven transits observed by *K2* is selected. The final dataset contains 194 photometric data points and 19 RV data points as listed in Table 2.

The datasets were fitted assuming a circular Keplerian orbit, i.e. we fixed eccentricity $e = 0$ and longitude of periastron $\omega = 90°$. Other orbital parameters were allowed to float, including the systemic velocity γ for the PARAS instrument, the RV semi-amplitude K, mid-transit time T_0, orbital period P_{orb}, impact parameter b, semi major axis in terms of stellar radius a/R_*, $q1$, $q2$, and the planet to star radius ratio R_p/R_*. Here, $q1$ & $q2$ are the parameterization of u_1 and u_2 as

---

[4] https://gea.esac.esa.int/archive/

described in Kipping (2013). Also, in order to fit the photometry data the quadratic limb-darkening law of Mandel & Agol (2002) was followed.

We generated 250,000 independent points for each free parameter by exploration of parameter space using 500 Markov chains. In order to find the global solution for the dataset, a wide range of uniform priors $P_{orb} = [19.40, 19.60]$ days, $T_0 = [2458112.5403, 2458114.6532]$, $b = [0, 1]$, $a/R_* = [5, 100]$, $R_p/R_* = [0.005, 0.1]$, $K = [0.001, 1.0]$ km s^{-1}, $\gamma_j = [1, 100]$ km s^{-1} and $q_1, q_2 = [0, 1]$ were chosen. The final derived parameter values and their associated uncertainties are given by the median and 68.3% confidence interval of the posterior probability distribution; these are listed in Table 4. The global fitting of the limb darkening coefficients gives $q_1 = 0.149^{+0.077}_{-0.075}$ & $q_2 = 0.457^{+0.384}_{-0.308}$, which results in $u_1 = 0.327^{+0.345}_{-0.231}$ & $u_2 = 0.028^{+0.220}_{-0.289}$. As the uncertainties associated with these are very high, we instead interpolate the limb darkening coefficients given in Claret & Bloemen (2011) for the Kepler-band, and also list these values in Table 4.
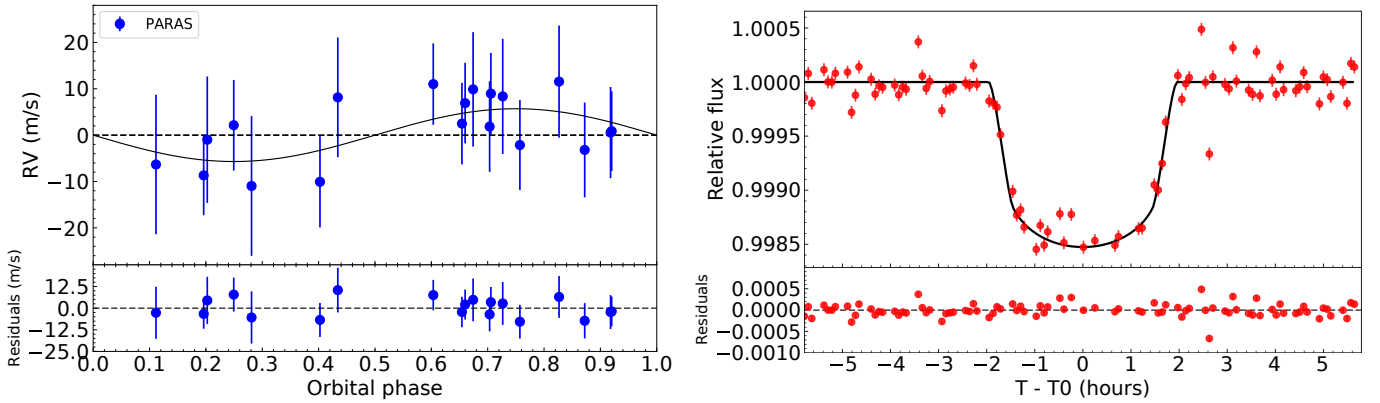

Figure 6. Left: RVs taken by PARAS, phased to the 19.491d period as determined from the simultaneous fitting of the photometric and RV data using `PYANETI`. The best fit model is also displayed together with the residuals. Right: Phase folded `K2PHOT` light curve centered on the T_0 with the best fit model in black overlaid.

Table 4. MEDIAN VALUES AND 68 % CONFIDENCE INTERVALS FOR THE LIGHCURVE AND RADIAL VELOCITY PARAMETERS OF THE EPIC 211945201 SYSTEM

Parameter	Units	Value
Stellar Parameters:		
M_*	Mass ($M_\odot$)....................	$1.18^{+0.03}_{-0.04}$
R_*	Radius ($R_\odot$)	$1.38^{+0.017}_{-0.018}$
ρ_*	Density (cgs)	$0.63^{+0.04}_{-0.03}$
$\log(g_*)$	Surface gravity (cgs)	4.25 ± 0.1
$T_{\rm eff}$	Effective temperature (K).......	6025 ± 100

Table 4 continued on next page

Table 4 *(continued)*

Parameter	Units	Value
[Fe/H]	Metallicity	0.1±0.1
Age	Gyr	$3.99^{+0.85}_{-0.7}$
Distance	pc	182.6±1.3
v_{micro}	Microturbulence (Km/s)	0.4±0.1
v_{rot}	Rotational Velocity (Km/s)	4.0±1.0
Planetary Parameters:Fitted		
T_0	Time of transit (BJD$_{\mathrm{TDB}}$)	$2458113.93994^{+0.00039}_{-0.00039}$
e	Eccentricity	0.0(fixed)
ω_*	Argument of periastron (degrees)	90.0(fixed)
P	Period (days)	$19.49213^{+0.00001}_{-0.00001}$
b	Impact Parameter...............	$0.85^{+0.007}_{-0.008}$
a/R_*	Semi-major axis in stellar radii ..	$23.10^{+0.47}_{-0.47}$
R_P/R_*	Radius of planet in stellar radii .	$0.0407^{+0.0003}_{-0.0003}$
K	RV semi-amplitude (m/s)	$5.7^{+3.0}_{-2.7}$
Planetary Parameters:Derived		
i	Inclination (degrees)	87.90±0.06
a	Semi-major axis (AU)..........	0.148±0.004
M_P	Mass ($M_\oplus$)	$27^{+14}_{-12.6}$
R_P	Radius ($R_\oplus$)	6.12±0.10
ρ_P	Density (cgs)	$0.65^{+0.34}_{-0.30}$
g_P	gravity(cgs)	$689.96^{+360.87}_{-322.20}$
T_P	Time of periastron (BJD$_{\mathrm{TDB}}$)...	$2458113.93994^{+0.00039}_{-0.00039}$
T_{eq}	Equilibrium Temperature (K)...	$886.35^{+17.36}_{-17.10}$
T_{23}	Total Eclipse duration (hours) ..	$2.92^{+0.04}_{-0.04}$
T_{14}	Total duration (hours)	3.91±0.02
Other Parameters:		
u_1	linear limb-darkening coeff	0.36[a]
u_2	quadratic limb-darkening coeff ..	0.29[a]
q_1	$(u_1 + u_2)^2$	0.42[a]
q_2	$u_1(2(u_1 + u_2))^{-1}$	0.28[a]
γ_{PARAS}	Systemic velocity (Km/s)	1.2588±0.0025

[a] Limb-Darkening coefficients obtained by interpolating the table of Claret & Bloemen (2011).

8. DISSCUSSION

The simultaneous fitting of RV and photometric data gives a RV semi-amplitude of $K = 5.7^{+3.0}_{-2.7}$ m s^{-1}, and mass of $M_p = 27^{+14}_{-12.6}$ $M_\oplus$ for EPIC 211945201b. This gives a 3-σ upper limit on the mass of 42 $M_\oplus$ above the nominal value. Leveraging the precision of the newly released GAIA DR2 data, the radius of the planet is derived to be 6.12±0.10 $R_\oplus$. This radius and mass correspond to a density of $0.65^{+0.34}_{-0.30}$ g cm^{-3}. It is be noted here that earlier radius estimates of $6.0^{+0.9}_{-0.8}$ $R_\oplus$ by Petigura et al. (2018) and $5.85^{+0.95}_{-0.78}$ $R_\oplus$ by Mayo et al. (2018) from Campaign 5 transit data alone; and 5.3 $R_\oplus$ by Yu et al. (2018) from Campaign 16 data, are in agreement with our simultaneous fitting results. The planet thus has a Saturn-like density while its mass and radius place it in the super-Neptune
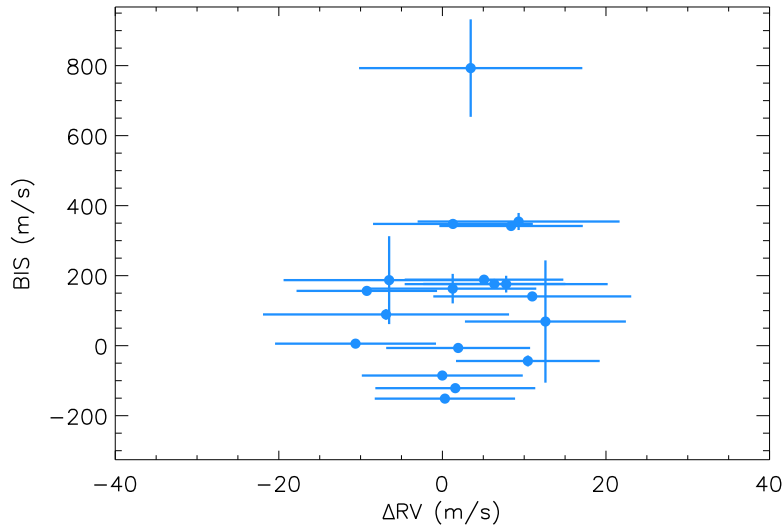
Figure 7. Distribution of measured radial velocities from PARAS, and associated values of the bisector inverse slope from the CCF. There is no significant correlation between the two, ruling out the possibility of blended spectra.

or sub-Saturn classification of exoplanets. This class of planets is currently very underpopulated (Bonomo et al. 2014).

EPIC 211945201b lies in the overlapping region between super-Neptunes and sub-Saturns. There are only 22 sub-Saturns in the range of 4-8 $R_\oplus$ whose mass and radius are precisely known, as discussed and listed in Table 7 of Petigura et al. (2017). In spite of the small range in radii, these planets are found to have a large mass range, and thus densities that vary between 2.40 to 0.26 g cm^{-3}, indicating diverse formation mechanisms (Bayliss et al. 2015). There is no obvious correlation between the radius and mass of these planets, making them an interesting class of exoplanets meriting further scrutiny.

The total transit duration time $T_{14,central}$, if the planet is passing in front of the stellar disk center, should be ∼6 hours using the equations of Seager & Mallén-Ornelas (2003). However, fitting the light curve (Sec 7) gives $T_{14} = 3.91$ hours, and an impact parameter of $b = 0.85$, suggesting that the planet is passing closer to the poles of the stellar disk. This indication of a grazing transit scenario likely results in the ∼2 % probability of an eclipsing binary in the VESPA output. However, the RV observations from PARAS conclusively rule out the EB scenario and confirm the planetary nature of the source.

We also estimate the internal composition of EPIC 211945201b using irradiated planetary composition models of Fortney et al. (2007) & Lopez & Fortney (2014). These are two layer partitioning models based on the assumption that planets are made up of a very dense core and a less dense envelope, and that all the heavy elements are concentrated in the core while the lighter elements are part of envelope. In Fig 8 we plot our results, along with the synthetic models used to estimate the core and envelope masses. The models chosen here are based on our final parameters for the EPIC 211945201 system – at an age of 3.16 Gyr and 0.1AU separation, with core masses of 0,10, and 25 $M_\oplus$ – where we interpolate between 10 and 25 $M_\oplus$ core mass models. We determine the heavy element content to be about 60-70% of the total mass. The non-irradiated models of Mordasini et al.

(2012) & Jin et al. (2014) were also used to find the heavy element fraction and the results found
to be consistent with 60-70%. However, we caution that these values have high uncertainties given
our errors on the planet density, and should be considered preliminary estimates until better mass
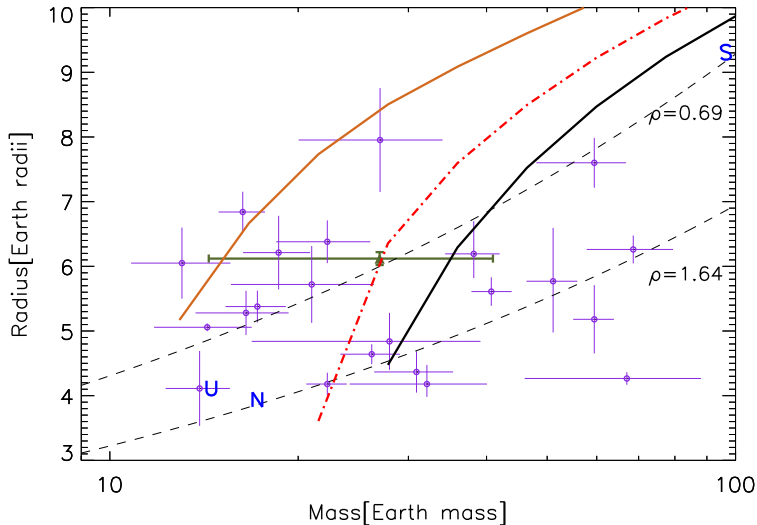measurements are obtained.

Figure 8. Mass versus radius diagram showing our measurements for EPIC 211945201b (olive trian-
gle). Overlaid are the theoretical curves for 3.16 Gyr and core masses of 10 and 25 $M_\oplus$ at 0.1 AU from
Fortney et al. (2007) in dark yellow and black, respectively. The dashed-dotted Red line is linearly interpo-
lated fortney model for core of 18 $M_\oplus$(see Sec 8). The dashed black lines from top to bottom are isodensity
curves for saturn & neptune density. The magenta coloured open circles represents the 22 superneptunes
($4.0 \leq R_\oplus \geq 8.0$, $10.0 \leq M_\oplus \geq 70.0$) whose mass and radius are determined with at least 50 % precision (from
http://exoplanet.eu/ , Schneider et al. 2011 & NASA exoplanet Archive, Akeson et al. 2013). The Blue
coloured U, N, and S represents here Uranus, Neptune and Saturn, respectively.

9. SUMMARY

We find strong evidence of a transiting sub-Saturn (or super-Neptune) around EPIC 211945201.
Previous work had deemed this a planetary candidate, which we validate with `VESPA` analysis. We
found the FPP for the planetary hypothesis to be >1%, with a ∼2 % probability that the system
is an EB. In order to resolve the situation, we conducted a campaign of high-resolution RV ob-
servations using the PARAS spectrograph. These RV measurements showed low dispersion over a
long time baseline, eliminating the EB scenario and confirming the planetary nature of the candi-
date. By simultaneously modeling the RV and *K2*-photometry data we derive a radius and mass of
6.12 ± 0.1 $R_\oplus$ and $27^{+14}_{-12.6}$ $M_\oplus$ for the companion. We then used the models of Fortney et al. (2007)
and Lopez & Fortney (2014) to make a notional prediction of the core mass, finding a substantial
projected heavy element fraction of 60-70 %, although more precise mass measurements are neces-
sary to confirm this heavy element content. EPIC 211945201b remains interesting as it straddles the
transition regime between ice giants and gas giants. The detection of similar exoplanets will continue
to hone our understanding of the formation and distribution of these worlds that have no analog in

our Solar System, and yet seem to abound in the nearby universe.

Future Works: The accurate mass of EPIC 211945201b can be determined with more precise RV measurements using HARPS (Pepe et al. 2003) or the newly-commissioned HPF (Mahadevan et al. 2014) spectrographs. This will provide clearer insight into the internal structure of the planet. The source is also a good target to study the star planet alignment (R-M effect) as the host star is relatively bright.

Software: VESPA (Morton 2012, Morton 2015), PARAS PIPELINE (Chakraborty et al. 2014), PARAS SPEC (Chaturvedi et al. 2016a,b), ISOCHRONES (Morton 2015), PYANETI (Barragán et al. 2016, 2017)

REFERENCES

Aigrain, S., Parviainen, H., & Pope, B. J. S. 2016, MNRAS, 459, 2408, doi: 10.1093/mnras/stw706

Akeson, R. L., Chen, X., Ciardi, D., et al. 2013, PASP, 125, 989, doi: 10.1086/672273

Baglin, A., Auvergne, M., Boisnard, L., et al. 2006, in COSPAR Meeting, Vol. 36, 36th COSPAR Scientific Assembly

Baranne, A., Queloz, D., Mayor, M., et al. 1996, A&AS, 119, 373

Barragán, O., Gandolfi, D., & Antoniciello, G. 2017, pyaneti: Multi-planet radial velocity and transit fitting, Astrophysics Source Code Library. http://ascl.net/1707.003

Barragán, O., Grziwa, S., Gandolfi, D., et al. 2016, AJ, 152, 193, doi: 10.3847/0004-6256/152/6/193

Barros, S. C. C., Demangeon, O., & Deleuil, M. 2016, A&A, 594, A100, doi: 10.1051/0004-6361/201628902

Bayliss, D., Hartman, J. D., Bakos, G. Á., et al. 2015, AJ, 150, 49, doi: 10.1088/0004-6256/150/2/49

Bonomo, A. S., Sozzetti, A., Lovis, C., et al. 2014, A&A, 572, A2, doi: 10.1051/0004-6361/201424617

Borucki, W. J., Koch, D., Basri, G., et al. 2010, Science, 327, 977, doi: 10.1126/science.1185402

Bouchy, F., Díaz, R. F., Hébrard, G., et al. 2013, A&A, 549, A49, doi: 10.1051/0004-6361/201219979

Bouchy, F., Pepe, F., & Queloz, D. 2001, A&A, 374, 733, doi: 10.1051/0004-6361:20010730

Chakraborty, A., Mahadevan, S., Roy, A., et al. 2014, PASP, 126, 133, doi: 10.1086/675352

Chaturvedi, P., Chakraborty, A., & Anandarao, B. G. 2016a, ArXiv e-prints. https://arxiv.org/abs/1610.07235

Chaturvedi, P., Chakraborty, A., Anandarao, B. G., Roy, A., & Mahadevan, S. 2016b, MNRAS, 462, 554, doi: 10.1093/mnras/stw1560

Claret, A., & Bloemen, S. 2011, A&A, 529, A75, doi: 10.1051/0004-6361/201116451

Crossfield, I. J. M., Ciardi, D. R., Petigura, E. A., et al. 2016, ApJS, 226, 7, doi: 10.3847/0067-0049/226/1/7

Cutri, R. M., & et al. 2013, VizieR Online Data Catalog, 2328

Cutri, R. M., Skrutskie, M. F., van Dyk, S., et al. 2003, 2MASS All Sky Catalog of point sources.

Díaz, R. F., Almenara, J. M., Santerne, A., et al. 2014, MNRAS, 441, 983, doi: 10.1093/mnras/stu601

Dotter, A., Chaboyer, B., Jevremović, D., et al. 2008, ApJS, 178, 89, doi: 10.1086/589654

Dressing, C. D., Vanderburg, A., Schlieder, J. E., et al. 2017, AJ, 154, 207, doi: 10.3847/1538-3881/aa89f2

Fortney, J. J., Marley, M. S., & Barnes, J. W. 2007, ApJ, 659, 1661, doi: 10.1086/512120

Gaia Collaboration, Katz, D., Antoja, T., et al. 2018, ArXiv e-prints. https://arxiv.org/abs/1804.09380

Hodapp, K. W., Jensen, J. B., Irwin, E. M., et al. 2003, PASP, 115, 1388, doi: 10.1086/379669

Howell, S. B., Sobeck, C., Haas, M., et al. 2014, PASP, 126, 398, doi: 10.1086/676406

Huber, D., Bryson, S. T., Haas, M. R., et al. 2016, ApJS, 224, 2, doi: 10.3847/0067-0049/224/1/2

Jin, S., Mordasini, C., Parmentier, V., et al. 2014, ApJ, 795, 65, doi: 10.1088/0004-637X/795/1/65

Kipping, D. M. 2013, MNRAS, 435, 2152, doi: 10.1093/mnras/stt1435

Kovács, G., Zucker, S., & Mazeh, T. 2002, A&A, 391, 369, doi: 10.1051/0004-6361:20020802

Lopez, E. D., & Fortney, J. J. 2014, ApJ, 792, 1, doi: 10.1088/0004-637X/792/1/1

Luger, R., Agol, E., Kruse, E., et al. 2016, AJ, 152, 100, doi: 10.3847/0004-6256/152/4/100

Mahadevan, S., Ramsey, L. W., Terrien, R., et al. 2014, in Proc. SPIE, Vol. 9147, Ground-based and Airborne Instrumentation for Astronomy V, 91471G

Mandel, K., & Agol, E. 2002, ApJL, 580, L171, doi: 10.1086/345520

Mayo, A. W., Vanderburg, A., Latham, D. W., et al. 2018, ArXiv e-prints. https://arxiv.org/abs/1802.05277

Mordasini, C., Alibert, Y., Georgy, C., et al. 2012, A&A, 547, A112, doi: 10.1051/0004-6361/201118464

Morton, T. D. 2012, ApJ, 761, 6, doi: 10.1088/0004-637X/761/1/6

—. 2015, VESPA: False positive probabilities calculator, Astrophysics Source Code Library. http://ascl.net/1503.011

Pepe, F., Mayor, M., Galland, F., et al. 2002, A&A, 388, 632, doi: 10.1051/0004-6361:20020433

Pepe, F., Rupprecht, G., Avila, G., et al. 2003, in Society of Photo-Optical Instrumentation Engineers (SPIE) Conference Series, Vol. 4841, Instrument Design and Performance for Optical/Infrared Ground-based Telescopes, ed. M. Iye & A. F. M. Moorwood, 1045–1056

Perruchot, S., Kohler, D., Bouchy, F., et al. 2008, in Proc. SPIE, Vol. 7014, Ground-based and Airborne Instrumentation for Astronomy II, 70140J

Petigura, E. A., Schlieder, J. E., Crossfield, I. J. M., et al. 2015, ApJ, 811, 102, doi: 10.1088/0004-637X/811/2/102

Petigura, E. A., Sinukoff, E., Lopez, E. D., et al. 2017, AJ, 153, 142, doi: 10.3847/1538-3881/aa5ea5

Petigura, E. A., Crossfield, I. J. M., Isaacson, H., et al. 2018, AJ, 155, 21, doi: 10.3847/1538-3881/aa9b83

Piskunov, N. E., & Valenti, J. A. 2002, A&A, 385, 1095, doi: 10.1051/0004-6361:20020175

Pope, B. J. S., Parviainen, H., & Aigrain, S. 2016, MNRAS, 461, 3399, doi: 10.1093/mnras/stw1373

Queloz, D., Henry, G. W., Sivan, J. P., et al. 2001, A&A, 379, 279, doi: 10.1051/0004-6361:20011308

Roy, A., Chakraborty, A., Mahadevan, S., et al. 2016, in Proc. SPIE, Vol. 9908, Ground-based and Airborne Instrumentation for Astronomy VI, 99086R

Schneider, J., Dedieu, C., Le Sidaner, P., Savalle, R., & Zolotukhin, I. 2011, A&A, 532, A79, doi: 10.1051/0004-6361/201116713

Seager, S., & Mallén-Ornelas, G. 2003, ApJ, 585, 1038, doi: 10.1086/346105

Torres, G., Fressin, F., Lissauer, J. J., et al. 2011, in Bulletin of the American Astronomical Society, Vol. 43, American Astronomical Society Meeting Abstracts #218, 112.06

Vanderburg, A., & Johnson, J. A. 2014, PASP, 126, 948, doi: 10.1086/678764

Wright, J. T., Roy, A., Mahadevan, S., et al. 2013, ApJ, 770, 119, doi: 10.1088/0004-637X/770/2/119

Yu, L., Crossfield, I. J. M., Schlieder, J. E., et al.
    2018, ArXiv e-prints.
    https://arxiv.org/abs/1803.04091